Article

Off-Target Inhibition of Human Dihydroorotate Dehydrogenase (hDHODH) Highlights Challenges in the Development of Fat Mass and Obesity-Associated Protein (FTO) Inhibitors

Marco Tarullo, Guillermo Fernandez Rodriguez, Alessia Iaiza, Sara Venezia, Alberto Macone, Alessio Incocciati, Silvia Masciarelli, Marcella Marchioni, Marta Giorgis, Marco Lucio Lolli, Federico Fornaseri, Ludovica Proietti, Florian Grebien, Serena Rosignoli, Alessandro Paiardini, Dante Rotili, Antonello Mai, Elena Bochenkova, Amedeo Caflisch, Francesco Fazi, and Alessandro Fatica*

Read Online

ACCESS | Metrics & More | Article Recommendations | Supporting Information

ABSTRACT: FTO, an N^6-methyladenosine (m^{6}A) and N^6,2′-O-dimethyladenosine (m^{6}A$_m$) RNA demethylase, is a promising target for treating acute myeloid leukemia (AML) due to the significant anticancer activity of its inhibitors in preclinical models. Here, we demonstrate that the FTO inhibitor FB23-2 suppresses proliferation across both AML and CML cell lines, irrespective of FTO dependency, indicating an alternative mechanism of action. Metabolomic analysis revealed that FB23-2 induces the accumulation of dihydroorotate (DHO), a key intermediate in pyrimidine nucleotide synthesis catalyzed by human dihydroorotate dehydrogenase (hDHODH). Notably, structural similarities between the catalytic pockets of FTO and hDHODH enabled FB23-2 to inhibit both enzymes. In contrast, the hDHODH-inactive FB23−2 analog, ZLD115, required FTO for its antiproliferative activity. Similarly, the FTO inhibitor CS2 (brequinar), known as one of the most potent hDHODH inhibitors, exhibited FTO-independent antileukemic effects. Uridine supplementation fully rescued leukemia cells from FB23-2 and CS2-induced growth inhibition, but not ZLD115, confirming the inhibition of pyrimidine synthesis as the primary mechanism of action underlying their antileukemic activity. These findings underscore the importance of considering off-target effects on hDHODH in the development of FTO inhibitors to optimize their therapeutic potential and minimize unintended consequences.

KEYWORDS: m^{6}A, m^{6}A$_m$, FTO, DHODH, FB23-2, brequinar
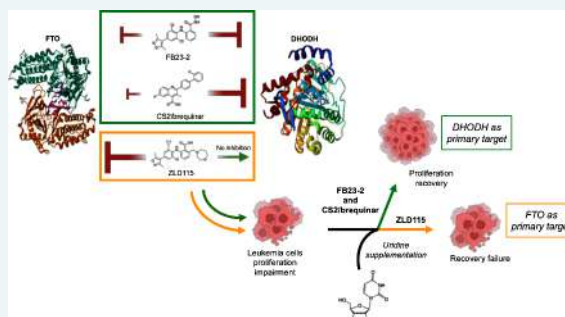
Accumulating evidence strongly correlates aberrant RNA modifications with cancer initiation, progression, and drug resistance.[1] Consequently, RNA-modifying enzymes have emerged as critical anticancer targets. Among the most significant RNA modifications in cancer is N^6-methyladenosine (m^{6}A) in mRNA.[2] In mammals, the nuclear METTL3−METTL14 complex is the principal writer of this modification,[3] with METTL3 catalyzing methylation and METTL14 essential for RNA binding.[3] Demethylation of m^{6}A modification is mediated by ALKBH5 (alkB homologue 5) and FTO (fat-mass and obesity-associated protein).[3] ALKBH5 exhibits high specificity for m^{6}A, while FTO acts on a broader range of modifications depending on its subcellular localization, including N^6,2′-O-dimethyladenosine (m^{6}A$_m$) at the cap, internal m^{6}A$_m$ within snRNAs, and N^1-methyladenosine (m^{1}A) within tRNAs (3). Notably, cytoplasmic FTO preferentially demethylates m^{6}A$_m$ at the cap rather than internal m^{6}A in mRNAs.[3]

FTO has emerged as a promising therapeutic target for acute myeloid leukemia (AML) due to its critical role in promoting leukemia cell survival, aerobic glycolysis, and inhibiting myeloid differentiation.[4−6] Notably, elevated FTO expression correlates with resistance to tyrosine kinase inhibitors (TKIs) and chemotherapeutic agents in both AML and chronic myeloid leukemia (CML).[6,7] Consequently, FTO inhibition has been shown to enhance the sensitivity of leukemia cells to these treatments.[7] Beyond hematological malignancies, FTO has also been implicated in the growth and drug resistance of various
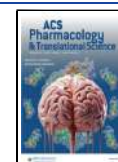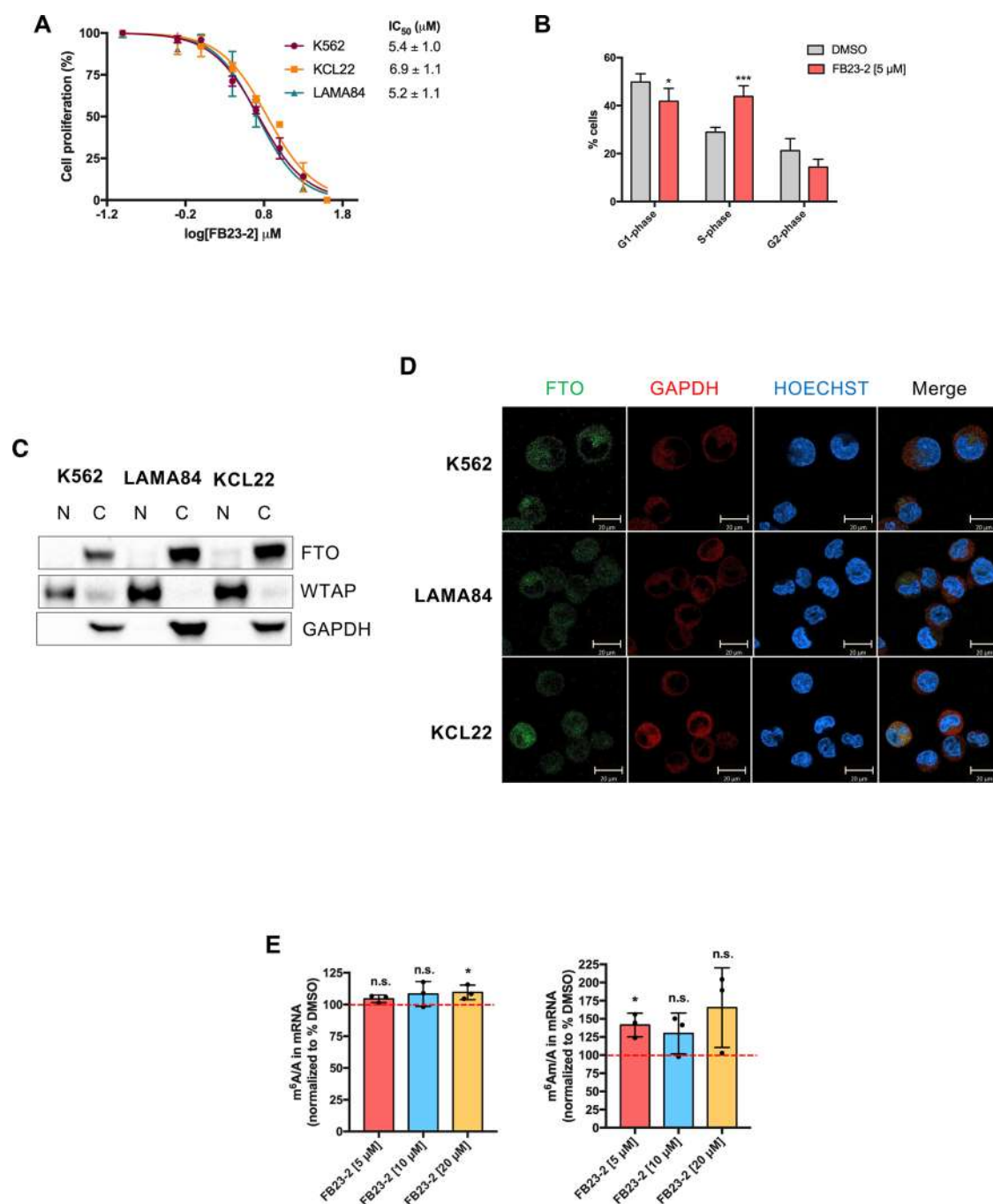
Figure 1. Antiproliferative effect of FB23-2 on CML cells is not mediated by increase in m^6A levels. (A) IC_{50} values of FB23-2 on inhibiting cell viability in K562, KCL22, and LAMA84 CML cell lines. The cells were treated for 72 h. (B) Histogram represents the cell cycle distribution of cells analyzed 48 h after 5 μM FB23-2 treatment. (C) Western blot analysis from nuclear (N) and cytoplasmic (C) fractions from the CML cell lines K562, LAMA84, and KCL22. GAPDH and WTAP indicate the cytosolic and nuclear compartment, respectively. (D) Immunofluorescence analysis of endogenous FTO in the CML cell lines K562, LAMA84, and KCL22. GAPDH and Hoechst indicate the cytosolic and nuclear compartment, respectively. (E) Quantitation of the percentage of m^6A/A (left panel) and m^6A_m/A ratios (right panel) in mRNA by LC-MS in K562 cells treated with 5, 10, and 20 μM of FB23-2 for 72 h. Data are normalized to the ratios of DMSO-treated cells (red dashed line).

solid tumors.[8] Given its pivotal role, substantial efforts have been dedicated to developing FTO inhibitors. FB23-2 and CS2 (brequinar) are highly effective small-molecule FTO inhibitors that demonstrate potent antileukemic activity in preclinical models.[9,10] FB23-2 has shown promise in targeting leukemia stem cells (LSCs), a critical cell population responsible for disease relapse.[9] Currently, FB23-2 is the most widely employed FTO inhibitor in preclinical studies.

In this investigation, we chose to further explore the antileukemic properties of FB23-2 and CS2/brequinar. We found that FB23-2 primarily inhibits human dihydroorotate dehydrogenase (hDHODH), which catalyzes the conversion of dihydroorotate (DHO) to rotate in the de novo pyrimidine biosynthesis pathway.[11] Inhibiting hDHODH depletes pyrimidines, depriving cells of essential nucleotides necessary for RNA and DNA synthesis. Our data show that FB23-2 affects both AML and CML cells regardless of their sensitivity to FTO
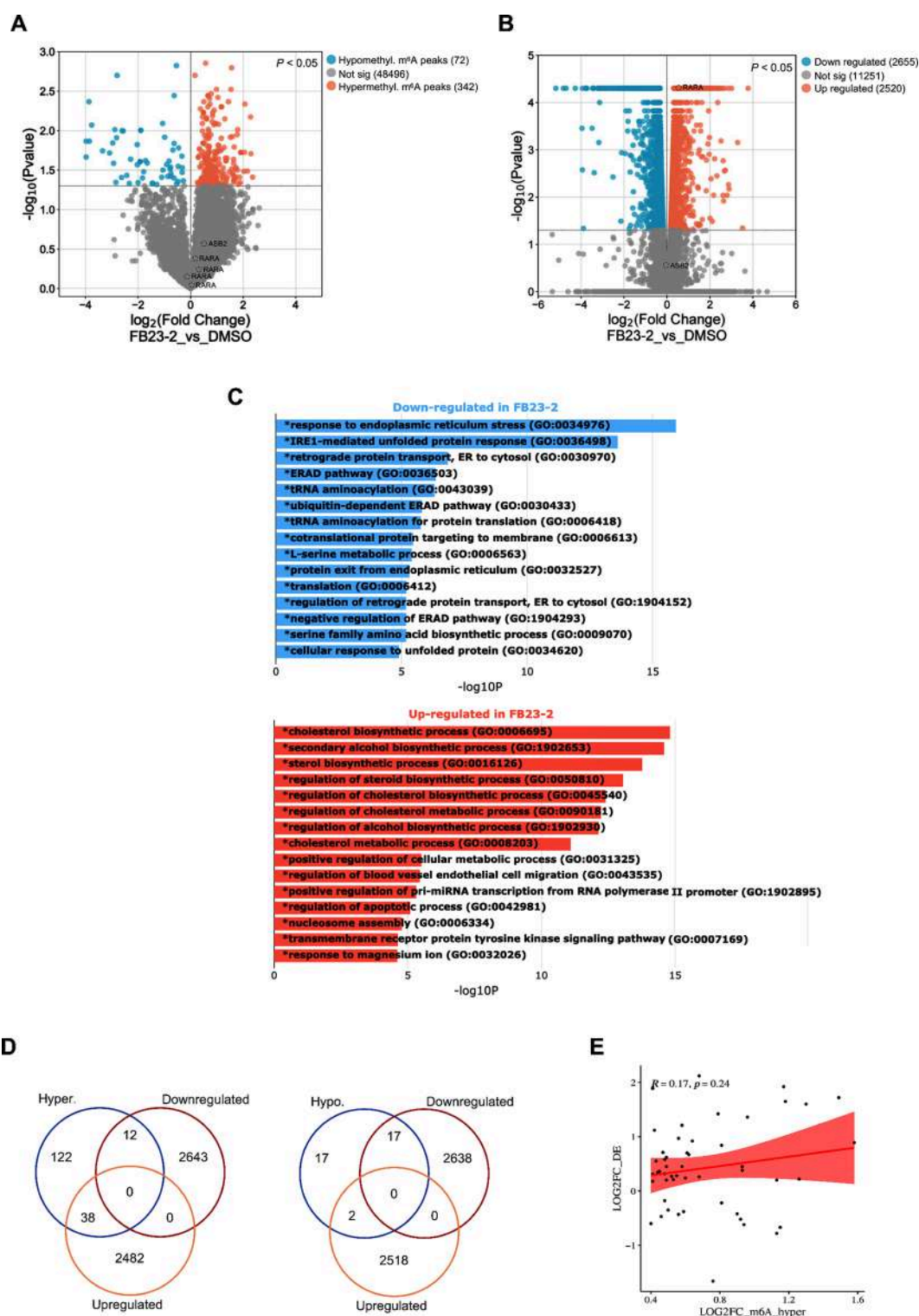
Figure 2. FB23-2 regulates mRNA levels independent of m⁶A modification. (A) Volcano plot showing the relationship between the fold-change and the significance of the differentially m⁶A methylated peaks in mRNA purified from K562 cells treated with 5 μM FB23-2 or DMSO. Gray dots represent peaks that are not significantly differentially methylated, while sky blue and orange dots are the genes that are significantly hyper- and hypo- methylated (absolute FC > 1), respectively. (B) Volcano plot showing the relationship between the fold change and the significance of the differential expression test for each gene in the genome. Gray dots represent the genes that are not significantly differentially expressed, while sky blue and orange dots are the genes that are significantly up- and down-regulated (absolute FC > 1), respectively. The FTO target genes RARA and ASB2 are indicated by black circles in both panels (A) and (B). (C) Gene Ontology Enrichment analysis results of differentially expressed genes upon FB23-2 treatment. The bar charts display the results of the Gene Ontology enrichment analysis performed on differentially expressed genes generated using Enrichr. The x axis indicates the −log10(P-value) for each term. Significant terms are highlighted in bold. (D) Overlap between significantly differentially expressed and m⁶A hypermethylated (Hyper.) and m⁶A hypomethylated (Hypo.) genes. (E) Pearson correlation between significantly differentially expressed (DE) and m⁶A hypermethylated genes (m⁶A-hyper.). Data are represented as mean ± SD, *P < 0.05, **P < 0.01, ***P < 0.001.
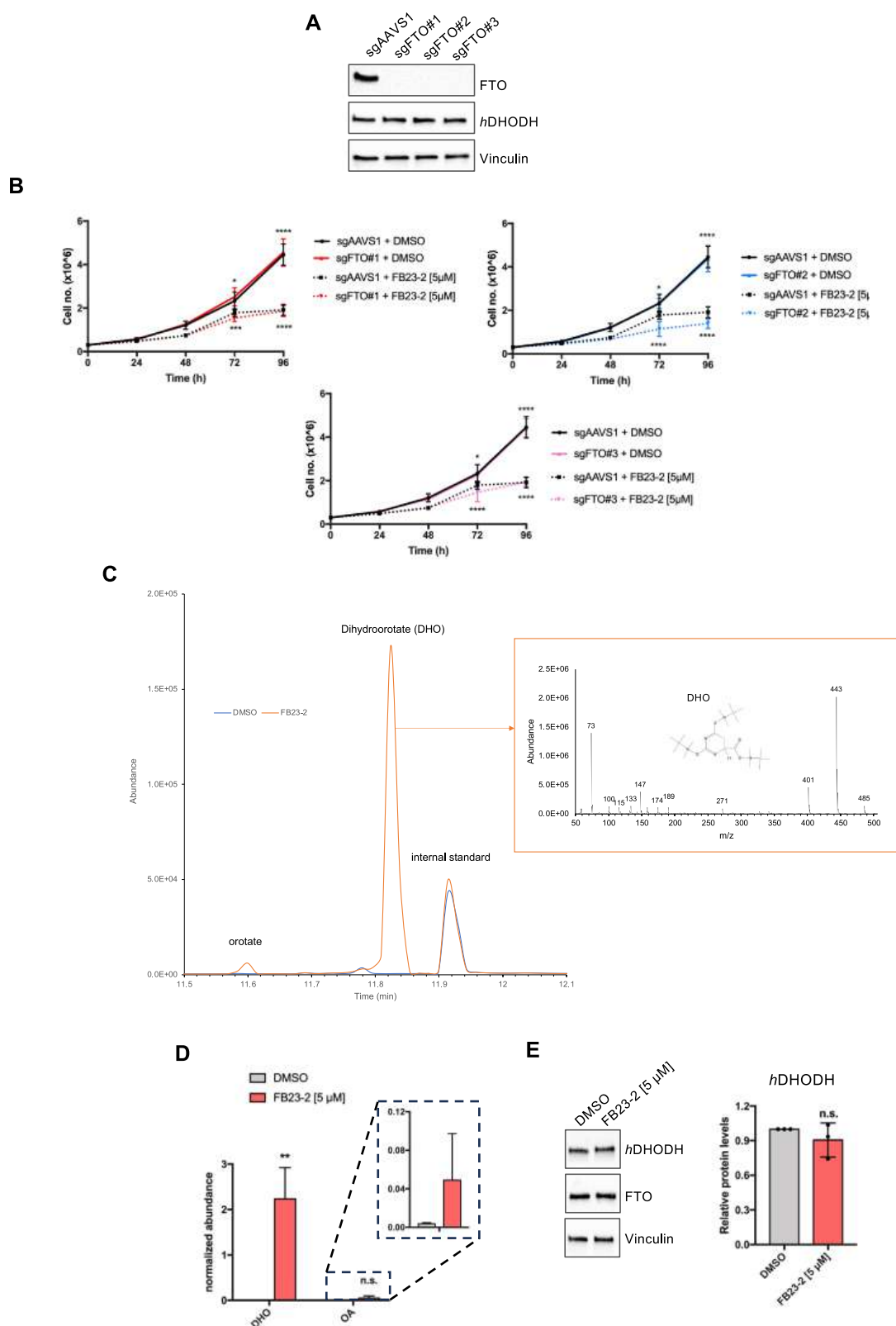
Figure 3. Antileukemic activity of FB23-2 is not attributable to the catalytic inhibition of FTO. (A) Western blot analysis of FTO, *h*DHODH, and vinculin protein levels in FTO knockout (sgFTO#1, sgFTO#2, and sgFTO#3) and control (sgAAVS1) K562 cell lines. (B) Growth curve of FTO knockout (sgFTO#1, sgFTO#2, and sgFTO#3) and control (sgAAVS1) K562 cell lines treated with 5 μM of FB23-2 or DMSO. (C) GC-MS chromatographic profile of K562 cells treated with 5 μM of FB23-2 or DMSO for 48 h. Chromatogram Electron ionization (EI) mass spectra of dihydroorotate (DHO) is shown in the frame. (D) The histograms represent the relative abundance of DHO and orotate (OA) measured by GC-MS in K562 cells treated with 5 μM of FB23-2 or DMSO. (E) Western blot analysis of FTO, *h*DHODH, and vinculin protein levels in K562 cells treated with 5 μM of FB23-2 or DMSO for 48 h. The histogram represents densitometric analysis of *h*DHODH/vinculin ratio from three independent experiments. Data are represented as mean $\pm$ SD, *$P < 0.05$, **$P < 0.01$, ***$P < 0.001$.

depletion. Additionally, we demonstrate that FB23-2 does not significantly impact m⁶A levels but affects m⁶A$_m$, with its antiproliferative effect fully rescued by adding exogenous uridine to the growth media. CRISPR/Cas9-mediated mutagenesis confirmed that FTO is dispensable, while *h*DHODH is required for the antileukemic activity of FB23-2. Thus, the antiproliferative action of FB23-2 is primarily due to the inhibition of *h*DHODH, not interference with FTO activity. In contrast, the FB23 analogue ZLD115,[12] which has a steric clash with the catalytic pocket of *h*DHODH, requires FTO for the antiproliferative effect. Supplementation with uridine does not help to rescue the antiproliferative activity of ZLD115. Notably, CS2/brequinar is one of the most potent inhibitors of *h*DHODH discovered so far.[13,14] We also demonstrated that FTO is dispensable for its activity and that adding uridine completely nullifies its antiproliferative effect on leukemia cells.[10] Our findings suggest that both FB23-2 and CS2 affect cell proliferation by primarily inhibiting *h*DHODH rather than FTO. Therefore, their use as selective FTO inhibitors should be avoided, and validation through uridine complementation assays is essential to demonstrate that their observed effects are not due to *h*DHODH inhibition. The structural homology of the catalytic pockets of *h*DHODH and FTO should also be considered in the design of future FTO inhibitors to avoid off-target effects.

■ RESULTS

Antiproliferative Effect of FB23-2 on Leukemia Cells Is Not Attributable to the Catalytic Inhibition of FTO. *FTO* is specifically upregulated in AML subtypes characterized by *MLL* rearrangements, *PML-RARA* and *RUNX1::RUNX1T1* translocations, internal tandem duplication of the *FLT3* gene (*FLT3-ITD*), and *NPM1* mutations.[4−6] FTO knockdown in cellular models derived from these AML subtypes, distinctly impacts cell proliferation and survival.[4−6] Conversely, the proliferation of CML cells is not significantly affected.[4] The FTO inhibitor FB23-2 exerts a potent inhibitory effect on the proliferation of AML cell lines with diverse genetic backgrounds and significantly diminishes the self-renewal of leukemia stem/initiating cells in mouse models.[9] Unexpectedly, FB23-2 also markedly reduced the proliferation of CML cell lines, showing similar antiproliferative effects as observed in FB23-2-sensitive AML cells (Figure 1A).[9] Cell cycle analysis of K562 cells treated with 5 μM FB23-2 revealed a significant arrest in the S-phase (Figures 1B and S1). Considering that FTO demethylase activity depends on its intracellular localization, we investigated its distribution in CML cell lines. Similar to previous observations in AML, the FTO protein was predominantly localized in the cytoplasm (Figure 1C,D), suggesting that FTO acts on m⁶A or m⁶A$_m$ levels in mRNAs. Despite the pronounced effect on proliferation arrest, global m⁶A levels in mRNA, measured by liquid chromatography−mass spectrometry (LC-MS), did not significantly increase in K562 cells treated with 5 or 10 μM FB23-2. Only a mild but significant increase was observed at 20 μM FB23-2 (Figure 1E). However, concentrations of FB23-2 exceeding 10 μM are not recommended due to reported off-target inhibition of diverse epigenetic regulators and kinases.[9] Conversely, m⁶A$_m$ methylation levels showed a more pronounced increase in all treatment conditions, although statistically significant at only 5 μM (Figure 1E). To further investigate these findings, we conducted an m⁶A-mRNA transcriptome microarray analysis to identify mRNAs exhibiting an increase in m⁶A levels in K562 cells treated with 5 μM FB23-2

compared to the DMSO control (Figure 2A). Consistent with the global methylation analysis, we observed only minor variations in m⁶A levels across the transcriptome. We identified 342 hypermethylated and 72 hypomethylated peaks corresponding to 172 and 36 genes, respectively (Table S1). Additionally, we performed RNA-seq on the same RNA samples to identify differentially expressed genes (Figure 2B). Bioinformatics analyses identified 2655 genes whose expression was downregulated by treatment with FB23-2, while the drug-induced the upregulation of 2520 genes (Table S2). The Gene Ontology (GO) analysis of differentially expressed genes showed that FB23-2 significantly downregulated biological processes involved in endoplasmic reticulum stress, unfolded protein response, and translation while upregulating biological processes involved in cholesterol, alcohol, and sterol biosynthetic processes (Figure 2C). A comparative analysis of RNA-seq data sets and m6A-mRNA transcriptome microarray data revealed a negligible overlap between transcripts whose expression is altered by FB23-2 treatment and those exhibiting differential m6A methylation (Figure 2D). Moreover, we did not observe any correlation between m⁶A hypermethylation, as expected by FTO inhibition, and the deregulation of individual mRNAs (Figure 2E). Notably, the FTO target genes, *RARA* and *ASB2*,[4] showed insignificant changes in m⁶A levels, whereas only RARA exhibits a significant yet modest alteration in gene expression (Figure 2A,B). These data indicate that the effect of FB23-2 on mRNA levels is linked neither to a global increase in m⁶A levels nor to a specific m⁶A increase in individual transcripts. However, we cannot exclude the possibility that the action of FB23-2 depends on the role of FTO in regulating m⁶A$_m$ mRNA levels.

The independence of the action of FB23-2 from FTO was confirmed by generating stable *FTO* knockout K562 cells through CRISPR/Cas9-mediated mutagenesis. We utilized three distinct single guide RNAs (sgRNAs) targeting the *FTO* gene in separate experiments, along with a control sgRNA targeting the *AAVS1* locus (Figure 3A). However, deletion of *FTO* in K562 cells had no discernible effect on cell proliferation when compared to the control sgRNA. Most importantly, FTO-deficient clones still exhibited a response to FB23-2 comparable to that of control cells (Figure 3B). These data indicate that the growth inhibition effect of FB23-2 on K562 CML cells is not attributable to the catalytic inhibition of FTO and implies alternative mechanisms of action for FB23-2.

Metabolomic Analysis Reveals Dihydroorotate (DHO) Accumulation and Rescue by Uridine in Leukemia Cells Treated with FB23-2. We conducted a metabolomic analysis using gas chromatography−mass spectrometry (GC-MS) to identify potential targets of FB23-2 in the K562 CML cells. We used FB23-2 at 5 μM, a concentration that significantly decreased cell proliferation (Figure 1A,B). Intriguingly, in cells treated with the FTO inhibitor, we observed a significant accumulation of dihydroorotate (DHO), which was barely detectable in the DMSO controls (Figure 3C). DHO is enzymatically converted by mitochondrial *h*DHODH into orotate (OA), a crucial intermediate for synthesizing uridine monophosphate (UMP) in the de novo pyrimidine synthesis pathway.[11] Quantitative analysis revealed a significant accumulation of DHO and, to a lesser extent, OA only in cells treated with FB23-2 (Figure 3D). Furthermore, *h*DHODH protein levels remained unchanged following FTO knockout (Figure 3A) or 5 μM FB23-2 treatment (Figure 3E), indicating that DHO accumulation is not due to a decline in *h*DHODH protein
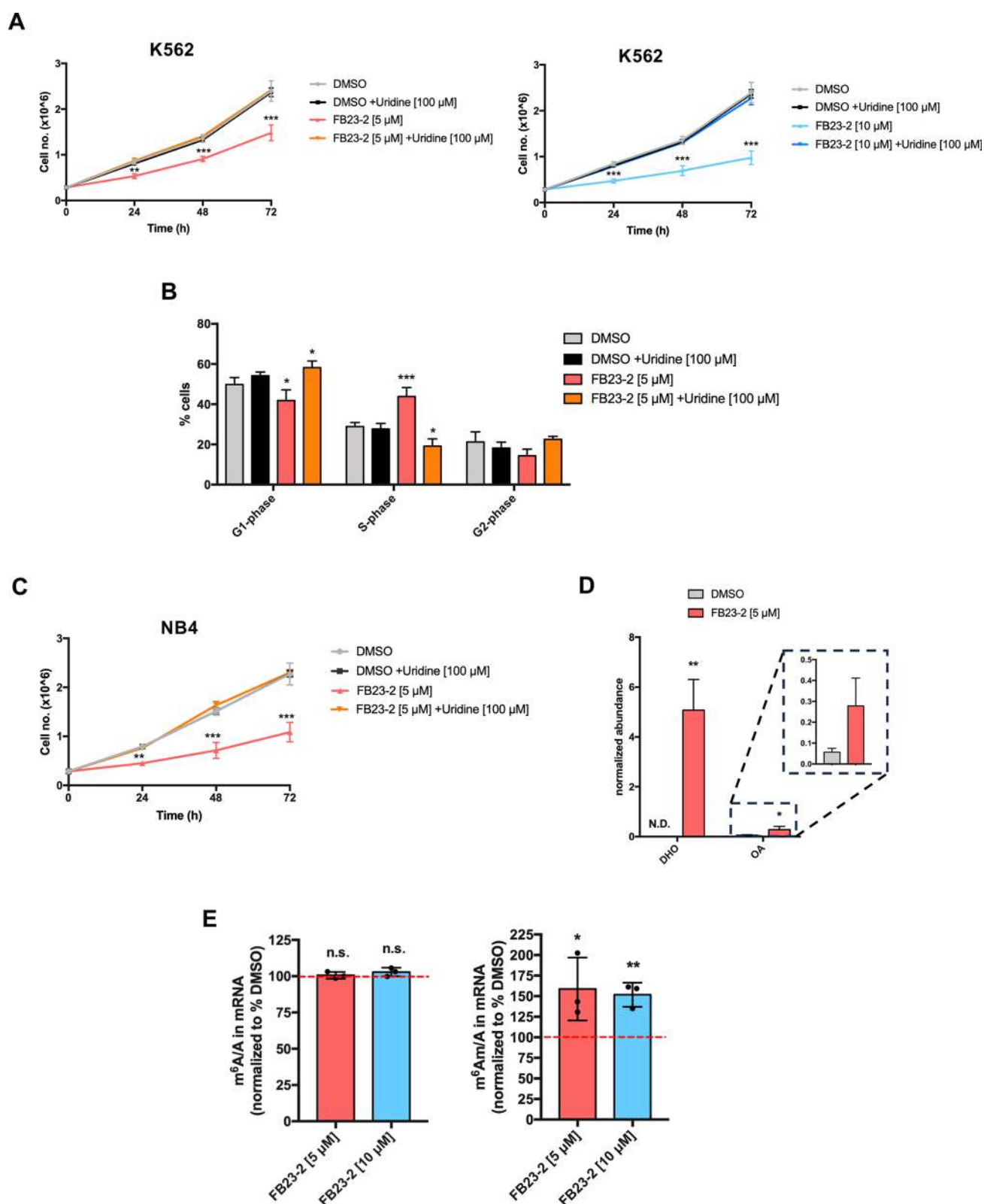
Figure 4. Antileukemic activity of FB23-2 is completely rescued by uridine complementation. (A) Growth curve of K562 cell line treated with different concentrations of FB23-2 (5 and 10 μM) or DMSO in the presence or absence of 100 μM uridine in the growth medium. (B) Upper panel, the histogram represents the cell cycle distribution of K562 cells analyzed 48 h after 5 μM FB23-2 treatment in the presence or absence of 100 μM uridine in the growth medium. Lower panel, representative cell cycle analysis. (C) Growth curve of NB4 cell line treated with 5 μM of FB23-2 or DMSO in the presence or absence of 100 μM uridine in the growth medium. (D) Histogram displaying the relative abundance of dihydroorotate (DHO) and orotate (OA) measured by GC-MS in NB4 cells treated with 5 μM of FB23-2 or DMSO. (E) Quantitation of the percentage of m^{6}A/A (left panel) and m^{6}A$_m$/A ratios (right panel) in mRNA by LC-MS/MS in NB4 cells treated with 5 μM of FB23-2 for 72 h. Data are normalized to the ratios of DMSO treated cells. Data are represented as mean $\pm$ SD, *$P < 0.05$, **$P < 0.01$, ***$P < 0.001$.
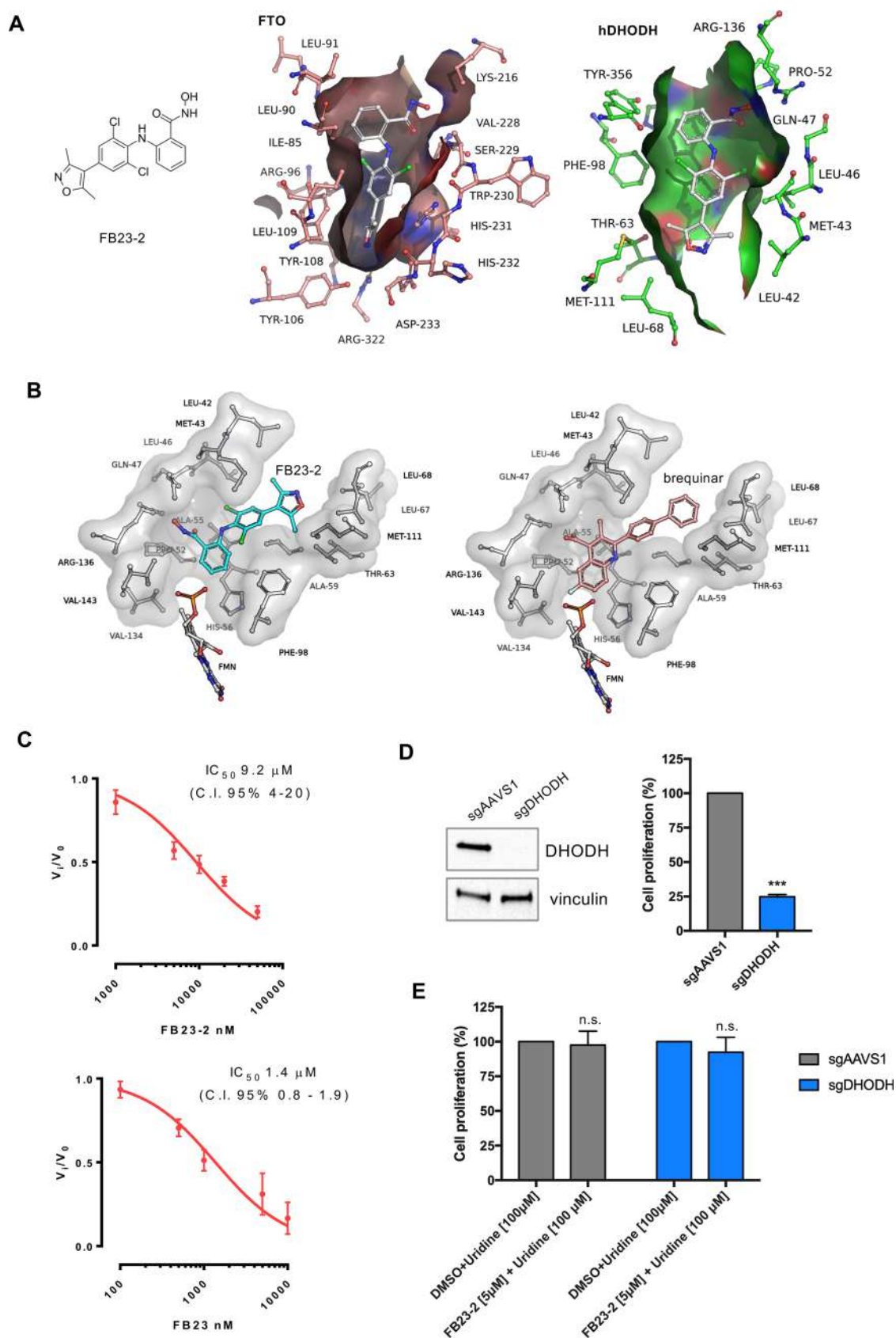
Figure 5. FB23-2 is a novel catalytic inhibitor of *h*DHODH. (A) Left panel, two-dimensional structure of FB23-2. Middle panel, FB23-2 bound to FTO is shown as gray sticks. The residues of the active site are labeled according to FTO (PDB: 6AKW). Right panel, FB23-2 bound to *h*DHODH is shown as gray sticks. *h*DHODH (PDB: 1D3G) active site is shown. Oxygen and nitrogen atoms colored in red and blue, respectively. (B) FB23-2 is shown as cyan sticks (left) and compared to (right) the crystal structure of a close brequinar analog (PDB: 1D3G). Oxygen and nitrogen atoms colored in red and blue, respectively. The residues of the active site are labeled according to *h*DHODH (PDB: 1D3G) and shown as sticks with a transparent

Figure 5. continued

surface. The position of flavin mononucleotide (FMN) is shown as reference. (C) Dose response curve of FB23-2, left panel, and FB23, right panel, obtained on recombinant hDHODH protein inhibition assay. (D) Left panel, Western blot analysis of hDHODH and vinculin protein levels in hDHODH knockout (sgDHODH) and control (sgAAVS1) K562 cell lines. Right panel, effect of hDODH knockout on the proliferation of K562 cells. Cell proliferation of hDHODH knockout is normalized to that of sgAAVS1 cells. (E) Effect of 72 h treatment of FB23-2 on proliferation of hDHODH KO K562 cells supplemented with uridine. Cell proliferation treated with FB23-2 is normalized to that treated with DMSO. Data are represented as mean $\pm$ SE of three independent experiments. *$P < 0.05$, **$P < 0.01$, ***$P < 0.001$, n.s. not significant.

levels. These data suggest that FB23-2 inhibits cellular hDHODH activity.

The disruption of orotate production, caused by hDHODH inhibition, can be rescued by supplementing the growth medium with uridine. Therefore, we analyzed the effect of FB23-2 on cell proliferation in the presence or absence of 100 μM uridine in the growth medium. Intriguingly, the effect of 5 and 10 μM FB23-2 was entirely nullified by the addition of uridine in K562 cells (Figure 4A). At these concentrations, the FTO inhibitor alone exhibited a profound effect on the K562 cell proliferation (Figure 3A). Cell cycle analysis confirmed that the S-phase arrest observed with 5 μM FB23-2 was completely reverted by the addition of uridine (Figures 4B and S1). These data further substantiate that FTO is not essential for the antiproliferative activity of FB23-2.

In view of these results, we chose to further explore the antileukemic properties of FB23-2 using the AML cell line NB4, whose proliferation is inhibited by FB23-2 at an IC$_{50}$ value of around 1 μM.[9,10] In this cell line, we also observed a complete restoration of cell proliferation upon the addition of uridine in the presence of 5 μM FB23-2 (Figure 4C). A significant accumulation of DHO was confirmed in NB4 cells treated with FB23-2 (Figure 4D). Notably, treatment with 5 and 10 μM of FB23-2 did not significantly alter the global m^{6}A/A ratio in NB4 mRNA, as measured by LC-MS (Figure 4E), consistent with the results from K562 cells. Interestingly, despite no significant change in the global m^{6}A/A ratio, FB23-2 treatment led to a marked increase in m^{6}A$_m$ levels, suggesting potential catalytic inhibition of FTO. However, this m^{6}A$_m$ accumulation appears unrelated to the antiproliferative effect of FB23-2, as uridine completely abolished the activity of the inhibitor.

These results demonstrate that the inhibition of proliferation by FB23-2 up to 10 μM in K562 cells and up to 5 μM in NB4 cells is primarily associated with the disruption of uridine synthesis and does not involve additional mechanisms unrelated to hDHODH inhibition, as the phenotype can be fully rescued by the addition of exogenous uridine.

FB23-2 Inhibits Human Dihydroorotate Dehydrogenase (hDHODH). Insights into the inhibition of hDHODH activity by FB23-2 were obtained through molecular docking simulations, which investigated the inhibitory potential of FB23-2 on hDHODH (Figure 5). Our results indicate that FB23-2 exhibits notable predicted binding affinity for hDHODH (PDB: 1D3G; predicted $\Delta G = -8.2$ kcal/mol), suggesting its ability to inhibit this enzyme in addition to its known inhibition of FTO (PDB: 6AKW). Furthermore, hDHODH and FTO have catalytic pockets with a similar shape and charge distribution (Figure 5A). In the FTO pocket, the hydroxamic moiety of FB23-2 makes hydrogen-bond contacts with Lys216 and Ser229, paralleled by Gln47 and Arg136 in hDHODH. The hydrophobic tail of FB23-2 is positioned within an apolar environment in both clefts, formed by Ile85, Leu90, Leu91, Leu109, and Val228 in FTO, and Leu42, Met43, Leu46, Leu68, Phe98, and Met111 in hDHODH. Comparative analysis of the

docking poses of FB23-2 and the crystal structure of the hDHODH inhibitor brequinar[13] bound to hDHODH highlighted similarities in their binding modes, further supporting the potential of FB23-2 as a dual inhibitor targeting both FTO and hDHODH (Figure 5B). We confirmed the inhibition of hDHODH by FB23-2 using an in vitro enzyme inhibition assay with recombinant hDHODH protein and DCIP as a colorimetric probe, the FB23-2 hDHODH inhibitor profile was confirmed (IC$_{50}$ = 9.2 μM; Figure 5C). To further validate the interaction between hDHODH and FB23-2 under cellular conditions, we performed a cellular thermal shift assay (CETSA). As anticipated, the presence of FB23-2 induced a discernible thermal shift of the hDHODH protein in K562 cells (Figure S2). Considering previously published data regarding the partial hydrolysis of FB23-2 to give its carboxylate derivative FB23 in cells and in rats[9] we decided to test also FB23 directly on isolated hDHODH protein and we observed an inhibitor activity once again (IC$_{50}$ = 1.4 μM; Figure 5C).

To confirm that the effect of FB23-2 is dependent on hDHODH, we generated an hDHODH knockout K562 line using CRISPR/Cas9. A guide against the *AAVS1* region was used as a control. As expected, hDHODH depletion significantly impacted the proliferative potential of the cells (Figure 5D). We then analyzed the effect of FB23-2 in wild-type (sgAAVS1) and hDHODH-depleted (sgDHODH) cells in the presence of uridine. Both wild-type and hDHODH knockout cells treated with FB23-2 exhibited growth identical to that of those treated with DMSO (Figure 5E). These findings corroborate that the antiproliferative effect of FB23-2 is attributed to the hDHODH inhibition.

FB23-2 was derived from FB23, which, despite its excellent enzymatic inhibition activity on FTO, exhibited poor cellular permeability.[9] Molecular docking simulations of the recently developed tricyclic benzoic acid analogue of FB23, ZLD115,[12] predicted a steric clash between the (1,4-Oxazepan-4-yl)-methyl group of ZLD115 and the hDHODH binding pocket (Figure 6A). We evaluated the antiproliferative effect of ZLD115 in K562 and NB4 cell lines. Consistent with expectations, ZLD115 exhibited a minimal impact on the proliferation of K562 cells, which are known to be insensitive to FTO depletion (Figure 5B). This observation supports the hypothesis that the antiproliferative effect of FB23-2 in K562 cells is solely due to hDHODH inhibition. Conversely, ZLD115 potently suppressed NB4 cell proliferation (Figure 6B). Notably, uridine supplementation failed to rescue the proliferative defect (Figure 6C), confirming an hDHODH-independent mechanism in these cells.

While FB23-2 uniquely exhibits off-target inhibition of hDHODH, its derivative ZLD115 remains selective for FTO. To address this potential insightful observation, we expanded our docking analysis to include other representative FTO inhibitors, not only derived from FB23, for which the experimentally determined complex with FTO is available (Table S3). For many of those FTO inhibitors, it was not
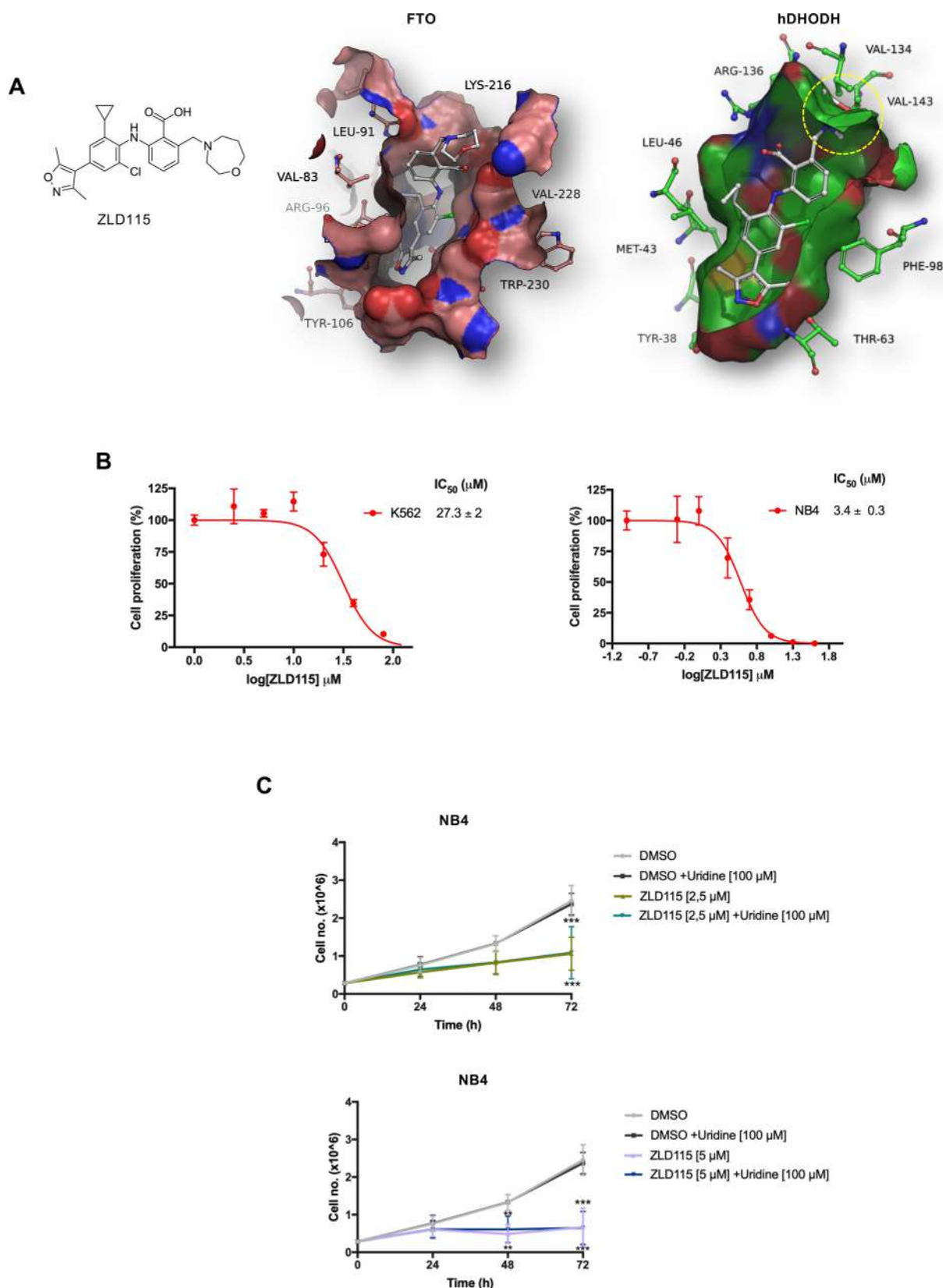
Figure 6. Selective FTO inhibitor ZLD115 does not target *h*DHODH (A) Left panel, two-dimensional structure of ZLD115. Predicted interaction mode of ZLD115 with human FTO (PDB: 6AKW) (middle) and *h*DHODH (PDB: 1D3G) (right). ZLD115 is shown as white sticks. Oxygen and nitrogen atoms colored in red and blue, respectively. The steric clash between the (1,4-Oxazepan-4-yl)-methyl group of ZLD115 and the binding pocket of DHODH (residues Val134 and Val143) is shown as a yellow dashed circle. (B) IC$_{50}$ values of ZLD115 on inhibiting cell proliferation in K562 (left panel) and NB4 cells (right panel). The cells were treated for 72 h. (C) Growth curve of NB4 cell line treated with 2.5 and 5 μM of ZLD115 or DMSO in the presence or absence of 100 μM uridine in the growth medium. Data are represented as mean $\pm$ SD, *$P < 0.05$, **$P < 0.01$, ***$P < 0.001$.
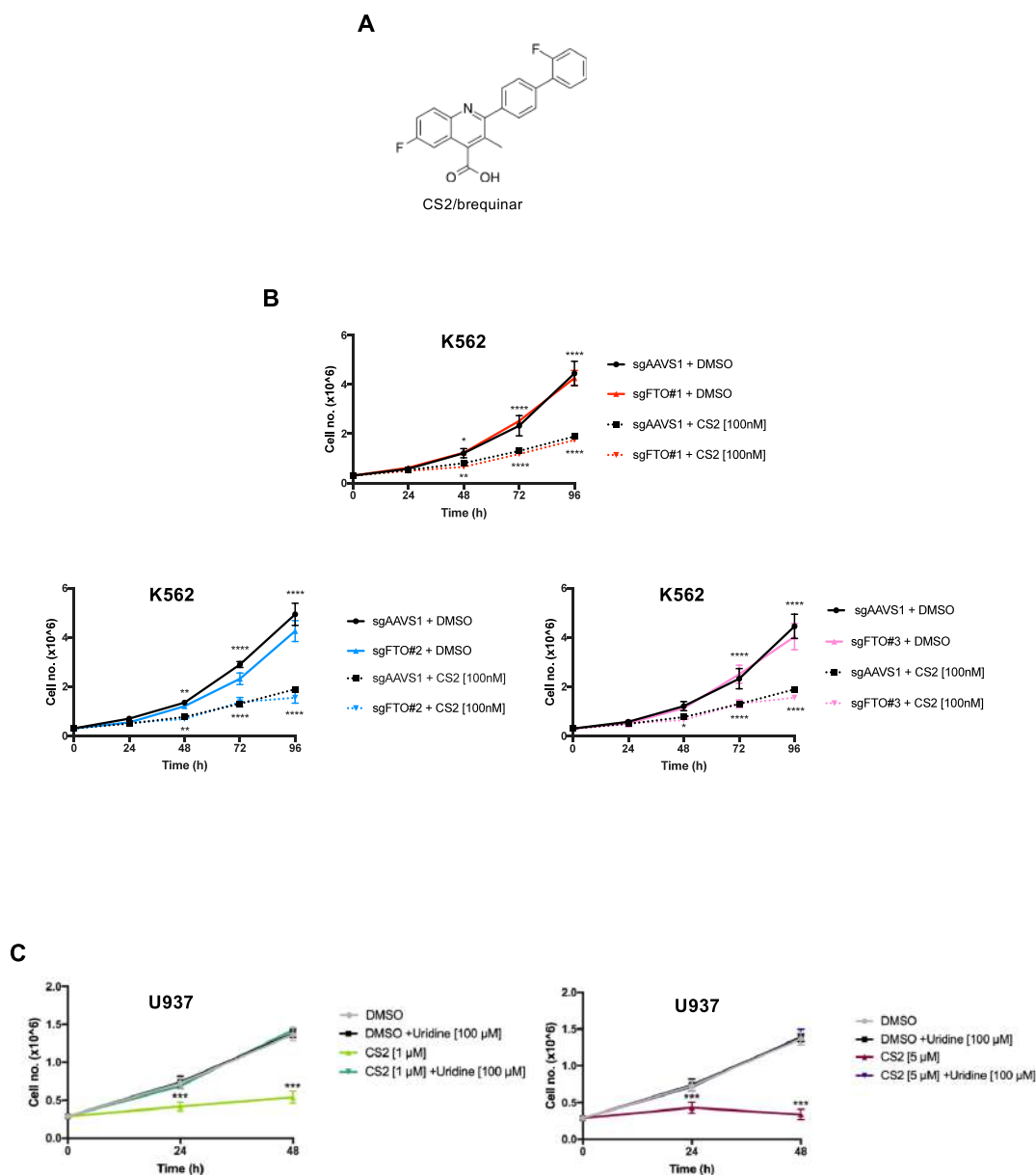
Figure 7. Antileukemic activity of CS2 is not attributable to the catalytic inhibition of FTO. (A) Two-dimensional structure of CS2/brequinar. (B) Growth curve of FTO knockout (sgFTO#1, sgFTO#2, and sgFTO#3) and control (sgAAVS1) cell lines treated with 100 nM of CS2 (brequinar) or DMSO. (C) Growth curve of U937 cell line treated with different concentrations of CS2 (1 and 5 μM) or DMSO in the presence or absence of 100 μM uridine in the growth medium. Data are represented as mean $\pm$ SD, *$P < 0.05$, **$P < 0.01$, ***$P < 0.001$.

possible to find a docked pose accommodating into the cleft of hDHODH in a conformation preventing severe steric clashes with the 20 Å × 10 Å cylinder-shaped cleft of hDHODH (Figure S3). From this structural analysis, we can conclude that not all of the FTO inhibitors are able to behave as dual inhibitors of FTO/ hDHODH. On the bulkiest compounds with moieties approaching Lys216 (e.g., ZL6 and 58W) and/or compounds interacting with the metal-binding cleft of FTO (e.g., NKG, HZX) are predicted to maintain their specificity for FTO. This expanded comparison will provide valuable insights into the design of future FTO inhibitors, helping to mitigate the risk of unintended hDHODH inhibition and thereby improving therapeutic specificity.

Antiproliferative Effect of CS2/Brequinar Is Independent of FTO Completely Rescued by Uridine Complementation. In light of these results, we investigated the

targeting of hDHODH using the second FTO inhibitor employed in preclinical studies, named CS2 (Figure 7A) (10). Indeed, CS2, previously identified as brequinar, is acknowledged as one of the most potent hDHODH inhibitors so far discovered.[12] Despite K562 cells not being affected by FTO knockdown (4) or knockout (Figure 3B), they still respond to the CS2 inhibitor.[10] Similar to FB23-2, FTO-deficient K562 cells exhibited an identical response to CS2 treatment as the controls (Figure 7B). This suggests that the action of CS2 in K562 cells is also independent of the presence of FTO. Previous studies have demonstrated the capacity of uridine to nullify the effects of hDHODH inhibitors, including CS2/brequinar, on AML cell lines.[15] Consistent with prior evidence, CS2/ brequinar demonstrated a robust effect on inducing cell growth arrest, even at nanomolar concentrations in the AML cell line U937.[10] However, the addition of uridine to the growth medium

completely rescued the growth defect phenotype that was induced by 1 and 5 μM of CS2/brequinar (Figure 7C), doses significantly higher than those required to inhibit FTO.[10] These data suggest that the antileukemic activity of CS2/brequinar is also attributable to the inhibition of hDHODH rather than FTO.

■ DISCUSSION

FTO overexpression has been implicated in various cancer types, including several AML subtypes, where it contributes to leukemia cell survival and drug resistance.[4−7] This has led to the development of FTO inhibitors exhibiting potent antitumor activity, particularly in AML models.[9,10] Our findings elucidate the mechanism underlying the antileukemic effects of the FTO inhibitors FB23-2 and CS2. Initially described as FTO inhibitors modulating m^{6}A levels,[9,10] our data demonstrate that their primary mode of action involves the inhibition of hDHODH, a critical enzyme in the de novo pyrimidine biosynthesis.[11]

Notably, we observed a more pronounced increase in m^{6}A$_m$ compared to m^{6}A levels in both CML and AML cells upon FTO inhibition. This finding aligns with recent studies demonstrating that FTO preferentially demethylates m^{6}A$_m$ over m^{6}A on mRNA.[16,17] Furthermore, we did not detect any correlation between m^{6}A levels and RNA expression levels upon FB23-2 treatment, including those of known FTO target genes, such as RARA and ASB2.[4] The significant accumulation of dihydroorotate (DHO) in FB23-2-treated cells, along with the rescue of the FB-23-2 induced proliferation defect by uridine supplementation, strongly suggests that the activity of this inhibitor is due to disrupting the de novo pyrimidine biosynthesis pathway rather than inhibiting FTO demethylases activity. This disruption leads to pyrimidine depletion, hindering essential nucleotide synthesis and causing cell cycle arrest in S-phase. A GO analysis of the biological processes influenced by FB23-2 in the K562 CML cell line revealed several pathways that converge with those identified following hDHODH inhibition in CML and other tumor types.[18−23] Notably, we observed a significant downregulation of translation and the unfolded protein response. The effect on translation is likely attributable to the depletion of UMP due to hDHODH inhibition, which subsequently leads to impaired rRNA synthesis and protein translation, ultimately limiting the growth and proliferation of cancer cells.[19,20] While the downregulation of the UPR is highly likely a consequence of reduced translation, which may prevent the accumulation of misfolded proteins, it can also reduce the stress resistance of cancer cells such as that induced by chemotherapeutic agents, leading to increased sensitivity to chemotherapy. We would also like to emphasize the parallelism between the pathways regulated by hDHODH and those modulated by changes in m^{6}A. Indeed, among the pathways influenced by FTO are translation and c-MYC-regulated genes,[4] both of which have been found to be downregulated following hDHODH inhibition.[18,21−23]

Molecular docking simulations and in vitro enzyme inhibition assays further support the dual inhibitory potential of FB23-2 against both FTO and hDHODH. The FTO-independence of FB23-2's antiproliferative effects and its dependence on hDHODH activity were corroborated using CRISPR/Cas9-mediated mutagenesis. Although hDHODH and FTO have distinct cellular functions, they exhibit catalytic pockets with similar shapes and charge distributions. The preferential targeting of hDHODH in vivo by FB23-2, despite comparable in vitro IC$_{50}$ values for FTO and hDHODH inhibition, warrants

further investigation. This discrepancy could be attributed to several factors related to the cellular environment. First, cellular compartmentalization might play a significant role, as FTO and hDHODH reside in distinct cellular compartments. FB23-2 might have differential accessibility to these enzymes within the cell. Interacting channel proteins, like VDAC3, which facilitates substrate channeling for hDHODH,[24] could influence FB23-2's ability to reach the hDHODH binding pocket more effectively in vivo. Second, differences in protein-drug interactions within the cellular environment compared to the in vitro assay might influence binding affinity. The intriguing cellular activity of FB23-2 and its ability, to directly translate hDHODH enzymatic inhibition into cellular effects within the same micromolar concentration range suggest that the compound is a critical factor in this phenomenon. As previously reported, lipophilicity is a critical determinant of cellular efficacy for hDHODH inhibitors due to the protein's mitochondrial localization.[25] A LogD7.4 value exceeding 2.5 is generally considered optimal for achieving substantial cellular effects. Unlike CS2/brequinar, which possesses a fully deprotonated carboxylate at physiological pH, FB23-2 involves a weak acidic hydroxamic moiety (pK_a ∼ 8) that could be considered neutral at physiological pH and a source of better membrane permeability. Moreover, the activity of FB23-2 could be reinforced and prolonged by the presence in cells of its still-active derivative FB23.[9] Interestingly, a similar discrepancy was observed for the hDHODH inhibitor PTC299 (emvododstat), which exhibited greater activity in cellular assays compared to in vitro enzymatic assays due to better penetrance in the mitochondria.[25]

Notably, CS2, formerly known as brequinar, has been previously characterized as one of the most potent hDHODH inhibitors,[13,26] inhibiting cellular proliferation at concentrations in the low nanomolar range.[27] The rescue of growth defects by uridine supplementation observed in AML cell lines sensitive to FTO knockdown is consistent with the established evidence of CS2/brequinar's impact on uridine synthesis.[13,26] Therefore, caution is warranted when attributing effects solely to FTO inhibition during CS2/brequinar use. Experiments employing this inhibitor should always incorporate uridine complementation assays to definitively exclude hDHODH inhibition, as it significantly impacts leukemia proliferation. Indeed, hDHODH inhibitors, exemplified by CS2/brequinar and emvododstat, demonstrated remarkable efficacy in preclinical models. These inhibitors are currently undergoing clinical evaluation for tumors dependent on the de novo pyrimidine nucleotide synthesis pathway, particularly, myeloid malignancies. To meet the demands of rapid DNA replication and cell proliferation, cancer cells frequently utilize de novo synthesis pathways, unlike normal cells, which primarily maintain nucleotide homeostasis through the nucleoside salvage pathway. However, intratumoral heterogeneity exists with some solid tumors exhibiting a continued reliance on the salvage pathway, contributing to the limited success of hDHODH-targeted therapies in clinical trials. Supplementation of uridine in the culture medium of cells treated with hDHODH inhibitors mimics the salvage pathway operating in vivo and effectively counteracts the hDHODH inhibition effect.

Our findings hold broader implications for interpreting past studies employing FB23-2 and CS2 as FTO inhibitors in leukemia.[9,10] These findings underscore the critical need for stringent validation during the FTO inhibitor development. Cell lines resistant to FTO inhibition, such as K562 cells, offer valuable tools to assess the selectivity of candidate FTO-specific

inhibitors. By analyzing these models, researchers gain insights into potential off-target effects, ultimately facilitating the development of more targeted cancer therapies. Considering *h*DHODH inhibition as an alternative mechanism of action is crucial. The FB23-2 analog, ZLD115,[12] exemplifies this concept. The structural alignment of the FB23-2 binding pockets of FTO and *h*DHODH shows that the FTO inhibitor ZLD115 does not fit sterically into *h*DHODH because of the 7-membered ring in ortho of the carboxyl group of FB23. Thus, bulky substituents in *ortho* of the hydroxamic acid of FB23-2 should improve the selectivity against *h*DHODH. Furthermore, besides hydroxamic acid, other isosteric replacements of the carboxyl moiety of FB23 might preserve its potency and improve its cell permeation.[28]

In conclusion, our study challenges the current understanding of FB23-2 and CS2 as selective FTO inhibitors, demonstrating their primary action on *h*DHODH. This refined understanding not only improves our knowledge of these compounds' mechanisms but also necessitates a reevaluation of their potential applications in future research.

■ MATERIALS AND METHODS

Cell Culture and Reagents. The leukemia cell lines K562 (CRL-3343, ATCC), KCL22 (a gift from Prof. Carlo Gambacorti-Passerini), LAMA84 (a gift from Prof. Carlo Gambacorti-Passerini), U937 (ACC-5, DSMZ), and NB4 (ACC-15, DSMZ) were cultured in RPMI 1640 supplemented with 10% heat-inactivated fetal bovine serum (FBS, Gibco Invitrogen, New York, USA), 2 mM L-Glutamine (Gibco Invitrogen, New York, USA), 100 U/mL penicillin (Gibco Invitrogen, New York, USA) and 100 μg/mL streptomycin (Gibco Invitrogen, New York, USA). The Lenti-X 293T cell line (Takara) was grown in DMEM medium with 10% FBS, 1 × L-Glutamine, 1 × penicillin−streptomycin. All cell lines were maintained at 37 °C under an atmosphere containing 5% CO$_2$. Cell lines were routinely tested for mycoplasma contamination with the LookOut Mycoplasma PCR Detection Kit (Merck KGaA, Darmstadt, Germany). FB23-2, FB23, CS2/brequinar, and ZLD115 were synthesized as previously described.[9,10,12] All compounds are >95% pure by HPLC analysis.

Cell Growth and Cell Cycle Analysis. Data for growth curves were obtained with the Countess 3 Automated Cell Counter (Thermo Fisher Scientific) and trypan blue staining. The cell cycle was analyzed by flow cytometry. Briefly, 8 × 10^5 cells were washed twice with PBS and then fixed with 70% ethanol for 24 h. Cells were then incubated for at least 3 h with 50 μg/mL propidium iodide (Sigma-Aldrich) and 50 units/mL Dnase-free RNase A (Sigma-Aldrich). After this step, cells were analyzed by using an Epics XL Cytometer (Beckman Coulter). Data were analyzed using Kaluza flow analysis software (Beckman Coulter).

Measurement of m^{6}A and m^{6}A$_m$ Levels by Ultra-performance Liquid Chromatography−Mass Spectrometry (UPLC-MS/MS). Total RNA was extracted using a Directzol RNA Miniprep kit (Zymo Research, Irvine, CA, USA) according to the manufacturer's instructions. PolyA$^+$ mRNA was isolated through two rounds of purification using Sera-Mag oligo(dT) magnetic beads (Cytiva) per sample. The polyadenylated RNA was eluted with nuclease-free water and its concentration was determined using NanoDrop; 100 ng of polyadenylated RNA was first decapped using RNA 5′ pyrophosphohydrolase (NEB) for 1 h according to the manufacturer's instructions and then digested to nucleosides and dephosphorylated in a one-pot reaction using 0.05 μL of the

nucleoside digestion mix (NEB) in 25 μL of the total reaction volume for 16 h at 37 °C. The samples were diluted 10-fold in solvent A (0.1% (v/v) formic acid in water) and subjected to nucleoside UPLC-MS/MS analysis at the Functional Genomics Centre Zurich, following previously described procedures.[29] All measurements were performed in technical duplicates and repeated in 3 biological replicates on different days.

Gas Chromatography−Mass Spectrometry (GC−MS). Dihydroorotate and orotate were analyzed by GC-MS as their TBDMS-derivatives. Cell pellets from three biological replicates of FB23-2- or DMSO-treated K562 and NB4 cells were resuspended in 0.1 mL of 0.1 M HCl/acetonitrile (1:1 vol/vol) solution. The samples were stirred (2 min), sonicated (1 min), and centrifuged (2 min at 4000 rpm). A 50 μL aliquot was then evaporated to dryness under a gentle stream of nitrogen, and 50 μL of neat MTBSTFA, followed by 500 μL of a solution of internal standard in acetonitrile (para-coumaric acid, 0.2 mg/mL), were added. The mixture was heated at 80 °C for 1 h. The sample was then neutralized with sodium bicarbonate and subjected to GC−MS analysis. GC−MS analyses were carried out with an Agilent 6850A gas chromatograph coupled to a 5973N quadrupole mass selective detector (Agilent Technologies, Palo Alto, CA, USA). Chromatographic separations were performed with an Agilent HP5 ms fused-silica capillary column (30 m × 0.25 mm i.d.) coated with 5%-phenyl-95%-dimethylpolysiloxane (film thickness 0.25 μm) as the stationary phase. Injection mode: splitless at a temperature of 250 °C. Column temperature program: 80 °C (1 min) ramped to 300 °C at a rate of 20 °C/min and held for 15 min. The carrier gas was helium at a constant flow of 1.0 mL/min. The spectra were obtained in the electron impact mode at 70 eV ionization energy; ion source 280 °C; ion source vacuum 10^{-5} Torr. The MS analysis was performed simultaneously in TIC (mass range scan from m/z 50 to 600 at a rate of 0.42 scans s^{-1}) and SIM mode. GC-SIM-MS analysis was performed by selecting the following ions: m/z 443 for dihydroorotate, m/z 441 for orotate, and m/z 335 for *para*-coumaric acid (internal standard).

Western Blot Assay. Cells were lysed with RIPA buffer and a fresh protease inhibitor cocktail (Roche). Lysates were quantified using the Bradford Assay Reagent (Thermo Fisher Scientific). A 25 μg portion of whole cell extract was separated by 4−15% SDS-PAGE with precast protein gels (Bio-Rad) and electroblotted to a nitrocellulose membrane (Advansta). Immunoblot analysis of nuclear and cytoplasmic fractions was performed as described previously.[30] Immunoblots were incubated with antibodies antivinculin (sc-73264; Santa Cruz Biotechnology), anti-FTO (ab92821, Abcam, USA) anti-WTAP 60188-1-Ig (Proteintech, Manchester, UK) anti-GAPDH BSM-33033M-HRP (Bioss, USA) and anti-*h*DHODH (sc-166348, Santa Cruz Biotechnology, USA). Detection was carried out with Clarity Western ECL Blotting Substrate (BioRad, Hercules, CA, USA) using the ChemiDocTM MP System and images were analyzed using Image LabTM Software (Bio-Rad).

CRISPR-Cas9-Based Knockout. sgRNAs were cloned into the LentiGuide-Puro-P2A-EGFP vector as previously described.[31] Leukemia cells were infected with Cas9-expressing lentivirus (lentiCas9-Blast)[32] and single clones were selected with 10 μg/mL blasticidin (GIBCO Invitrogen, New York, USA). Then, Cas9-expressing single-cell clones were infected with sgRNA-expressing lentivirus carrying either lentiGuide-Puro-sgFTO, lentiGuide-Puro-sgDHODH or lentiGuide-Puro-sgAAVS1 and the sgRNA-transduced cells were subjected to puromycin selection (1 μg/mL). Cas9- and sgRNA-expressing

lentivirus were generated by cotransfection of the second-generation package plasmids pMD2.G and psPAX2 into Lenti-X 293T cells (Takara) in a 60 mm cell culture dish with calcium phosphate transfection. The calcium phosphate−DNA precipitate was allowed to stay on the cells for 14−16 h, after which the medium was replaced with a complete medium supplemented with 1 mM sodium butyrate (Sigma-Aldrich). The medium was collected 48 h after transfection, centrifuged at 1000 rpm for 5 min at room temperature, and filtered through 0.45 μm pore nitrocellulose filters. Cells were transduced by spinoculation.

gRNA targeting sequences are FTO#1, 5′-CGGTGGGTGGAACTAAACCG-3′; FTO#2, 5′-GTTTAGTTCCACCCACCGAG-3′; FTO#3, 5′-GAAGC-GAACAGCCAGTCTGT-3′; DHODH, 5′-GAAGCGAA-CAGCCAGTCTGT-3′; AAVS1 see.[16]

m6A-mRNA Epitranscriptomic Microarray. m^{6}A modification levels were quantified using the Arraystar Human m6A-mRNA&lncRNA Epitranscriptomic microarray (Arraystar) based on Arraystar's standard protocols. Briefly, the total RNAs were immunoprecipitated with the anti-N^6-methylade-nosine (m^{6}A) antibody (Synaptic Systems, Goettingen, Germany). The modified RNAs were eluted from the immunoprecipitated magnetic beads as the "IP". The unmodified RNAs were recovered from the supernatant as "Sup". The "IP" and "Sup" RNAs were labeled with Cy5 and Cy3, respectively, as cRNAs in separate reactions using Arraystar RNA Labeling protocol. The cRNAs were combined and hybridized onto the Arraystar Human mRNA&lncRNA Epitranscriptomic Microarray (8 × 60K, Arraystar). After washing the slides, the arrays were scanned in two-color channels by an Agilent Scanner G2505C. Agilent Feature Extraction software (version 11.0.1.1) was used to analyze acquired array images. Raw intensities of IP (immunoprecipitated, Cy5-labeled) and Sup (supernatant, Cy3-labeled) were normalized with an average of log2-scaled Spike-in RNA intensities. After Spike-in normalization, the probe signals having Present (P) or Marginal (M) QC flags in at least 1 out of 6 samples were retained for further "m6A quantity" analyses. "m6A quantity" was calculated for the m6A methylation amount based on the IP (Cy5-labeled) normalized intensities. Differentially m6A-methylated RNAs between two comparison groups were identified by filtering with the fold change and statistical significance thresholds (P value <0.05).

RNA Sequencing. Total RNA was extracted using the Directzol RNA Miniprep kit (Zymo Research, Irvine, CA, USA) according to the manufacturer's instructions. Total RNA from triplicates was sent to Procomcure Next Generation Sequencing (NGS; Vienna, AT) for library preparation using the Nextflex Rapid Directional RNA-Seq kit 2.0 (PerkinElmer, Waltham, MA, USA) and subjected to sequencing (2 × 150 bp paired-end) on an Illumina Novaseq 6000 system (Illumina, San Diego, CA, USA). The RNA-seq data were analyzed with the Artificial Intelligence RNA-seq Software as a Service (SaaS) platform (https://transcriptomics.cloud), as described.[30] DESeq2 software was then used for the identification of differentially expressed genes.[33] Genes were considered differentially expressed if the adjusted P value of the logarithm of the fold change was less than or equal to 0.05. Enrichment results were generated by analyzing the up-regulated and down-regulated gene sets using Enrichr.[34] Significant terms are determined by using a cutoff of P value <0.05 after applying the Benjamini−Hochberg correction.

Molecular Modeling. Molecular docking of FB23-2 and ZLD115 to hDHODH (PDB: 1D3G) was carried out by using Vina, as implemented in DockingPie.[35] A 5 Å × 5 Å × 5 Å box centered on BRE (2-BIPHENYL-4-YL-6-FLUORO-3-METH-YL-QUINOLINE-4-CARBOXYLIC ACID) was used as the energy grid. Ten independent simulations were carried out, and the pose with the lowest energy was accepted.

hDHODH Inhibition Assay. Following the procedure described in a previous study,[36] the plasmid pFN2A-hDHODH was utilized for the expression of N-terminal GST-tagged human hDHODH in BL21 (DE3) *Escherichia coli* cells; in the following, the protein was purified as previously described. Inhibitory activity was then assessed by monitoring the reduction of 2,6-dichloroindophenol (DCIP), which is associated with the oxidation of dihydroorotate catalyzed by the hDHODH enzyme. The enzyme was preincubated for 5 min at 37 °C in a Tris-buffer solution (pH 8.0) with coenzyme Q10 (100 μM), FB23-2 at different concentrations (final DMSO concentration 0.1% v/v), and DCIP (50 μM). The reaction was initiated by the addition of DHO (500 μM) and the reduction was monitored at λ = 650 nm. The initial rate was measured in the first five min (ε = 10,400 M^{-1} cm^{-1}) and the IC$_{50}$ value was calculated starting from V_i/V_0 (i = inhibitor; 0 = control) values from three independent experiments using GraphPad Prism software.

Immunofluorescence. Immunofluorescence was performed as previously described.[30] Cells were washed with PBS and fixed with a 4% formaldehyde solution (Sigma-Aldrich) for 10 min at room temperature. After permeabilization with 0.1% Triton X-100 (Sigma-Aldrich) for 10 min, cells were blocked with 3% bovine serum albumin (BSA) for 1 h and incubated with the primary antibodies anti-FTO (ab92821, Abcam) and anti-GAPDH (TA802519, OriGene) overnight at 4 °C. After two washes with Perm/Wash buffer (no. 554723, Becton Dickinson), cells were incubated with the secondary antibodies Alexa Fluor 555-labeled goat antimouse (#A-21422, Invitrogen) and Alexa Fluor 488-labeled goat antirabbit (A-11034, Invitrogen). The nuclei were stained with Hoechst 33342 (Life Technologies) for 5 min in a Perm/Wash buffer. Cells were then mounted in a VECTASHIELD antifade mounting media (H-1000, Vector Laboratories, Newark, CA, USA). Images were acquired using an LSM 900 confocal laser scanning microscope (Zeiss, Munich, Germany).

Cell Thermal Shift Assay (CETSA). CETSA was performed following the previously described protocol.[37] K562 cells were harvested in PBS supplemented with a protease inhibitor cocktail (complete, EDTA-free, Roche). The cell suspensions were freeze−thawed three times in liquid nitrogen and then centrifuged at 20,000g for 20 min at 4 °C. The lysates were divided into two aliquots and treated with DMSO or 50 μM of FB23-2, respectively. After incubation at room temperature for 30 min, the lysates were divided into equal parts (50 μL) and heated individually at different temperatures for 3 min. The heated samples were cooled to room temperature for 3 min and centrifuged at 20,000g for 20 min at 4 °C. The supernatants were transferred to new tubes and analyzed by Western blotting.

Statistical Analysis. Cell growth was analyzed by two-way analysis of variance (ANOVA) using Dunnett's multiple comparison test, and Western blot and immunofluorescence analysis were conducted using one-way ANOVA using Tukey's multiple comparison test. All statistical tests were performed using GraphPad Prism 8 software (GraphPad Software, San Diego, CA, USA). Analyses were performed from at least three

independent replicates ($n \geq 3$). A P value <0.05 was considered statistically significant.

ASSOCIATED CONTENT

Data Availability Statement

The RNA-sequencing data set has been deposited in ArrayExpress (accession number E-MTAB-11751) and the human m6A-mRNA&lncRNA Epitranscriptomic microarray data set in GEO (accession number GSE254577).

Supporting Information

The Supporting Information is available free of charge at https://pubs.acs.org/doi/10.1021/acsptsci.4c00533.

> Cell cycle analysis of FB23-2 treated K562 cells; CETSA assay with hDHODH in K562 cells; and superposed three-dimensional structures of representative FTO-inhibitors solved in complex with FTO (PDF)

> Differential m^{6}A levels in FB23-2_vs_DMSO K562 treated cells; differentially expressed genes in FB23-2 vs DMSO K562 treated cells (PDF)

AUTHOR INFORMATION

Corresponding Author

Alessandro Fatica − *Department of Biology and Biotechnologies "Charles Darwin", Sapienza University of Rome, 00185 Rome, Italy;* orcid.org/0000-0002-0743-7905; Email: alessandro.fatica@uniroma1.it

Authors

Marco Tarullo − *Department of Biology and Biotechnologies "Charles Darwin", Sapienza University of Rome, 00185 Rome, Italy*

Guillermo Fernandez Rodriguez − *Department of Biology and Biotechnologies "Charles Darwin", Sapienza University of Rome, 00185 Rome, Italy*

Alessia Iaiza − *Department of Biology and Biotechnologies "Charles Darwin", Sapienza University of Rome, 00185 Rome, Italy*

Sara Venezia − *Department of Biology and Biotechnologies "Charles Darwin", Sapienza University of Rome, 00185 Rome, Italy*

Alberto Macone − *Department of Biochemical Sciences "A. Rossi Fanelli", Sapienza University of Rome, 00185 Rome, Italy;* orcid.org/0000-0003-0455-1400

Alessio Incocciati − *Department of Biochemical Sciences "A. Rossi Fanelli", Sapienza University of Rome, 00185 Rome, Italy*

Silvia Masciarelli − *Department of Anatomical, Histological, Forensic & Orthopedic Sciences, Section of Histology & Medical Embryology, Sapienza University of Rome, 00161 Rome, Italy*

Marcella Marchioni − *Institute of Biology, Molecular Medicine and Nanobiotechnology, CNR, Sapienza University of Rome, 00185 Rome, Italy*

Marta Giorgis − *Department of Drug Science and Technology, University of Torino, 10125 Torino, Italy;* orcid.org/0000-0002-3282-1220

Marco Lucio Lolli − *Department of Drug Science and Technology, University of Torino, 10125 Torino, Italy;* orcid.org/0000-0002-3030-3163

Federico Fornaseri − *Department of Drug Science and Technology, University of Torino, 10125 Torino, Italy*

Ludovica Proietti − *Institute of Medical Biochemistry, University of Veterinary Medicine, 1210 Vienna, Austria*

Florian Grebien − *Institute of Medical Biochemistry, University of Veterinary Medicine, 1210 Vienna, Austria; St. Anna Children's Cancer Research Institute (CCRI), 1090 Vienna, Austria; CeMM Research Center for Molecular Medicine of the Austrian Academy of Sciences, 1090 Vienna, Austria*

Serena Rosignoli − *Department of Biochemical Sciences "A. Rossi Fanelli", Sapienza University of Rome, 00185 Rome, Italy*

Alessandro Paiardini − *Department of Biochemical Sciences "A. Rossi Fanelli", Sapienza University of Rome, 00185 Rome, Italy*

Dante Rotili − *Department of Science, Roma Tre University, 00146 Rome, Italy;* orcid.org/0000-0002-8428-8763

Antonello Mai − *Department of Drug Chemistry and Technologies, Sapienza University of Rome, 00185 Rome, Italy;* orcid.org/0000-0001-9176-2382

Elena Bochenkova − *Department of Biochemistry, University of Zurich, CH-8057 Zürich, Switzerland*

Amedeo Caflisch − *Department of Biochemistry, University of Zurich, CH-8057 Zürich, Switzerland;* orcid.org/0000-0002-2317-6792

Francesco Fazi − *Department of Anatomical, Histological, Forensic & Orthopedic Sciences, Section of Histology & Medical Embryology, Sapienza University of Rome, 00161 Rome, Italy*

Complete contact information is available at:
https://pubs.acs.org/10.1021/acsptsci.4c00533

Author Contributions

Investigation, M.T., G.F.R., A.I., S.V., M.M., A.M., M.G., E.B., A.P.; Resources, L.P., D.R., A.M.; Formal Analysis, M.T., G.F.R, A.I., S.R., A.P., A.F.; Visualization, M.T., G.F.R., A.I., S.R., A.P., A.F., Supervision, F.G., M.L.L., A.C., S.M., F.F., A.F.; Conceptualization, A.F.; Writing−Original Draft, A.F.; Funding Acquisition, F.F and A.F.; M.T. and G.F.R. contributed equally.

Notes

The authors declare no competing financial interest.

ACKNOWLEDGMENTS

ABBREVIATIONS

AML, acute myeloid leukemia; ALKBH5, alkB homologue 5; ASB2, Ankyrin Repeat And SOCS Box Containing 2; CML, chronic myeloid leukemia; DHO, dihydroorotate; FMN, flavin mononucleotide; FLT3-ITD, internal tandem duplication of

FLT3 gene; FTO, fat-mass and obesity-associated protein; GC-MS, gas chromatography−mass spectrometry; GO, Gene Ontology; hDHODH, human dihydroorotate dehydrogenase; IC_{50}, half maximal inhibitory concentration; LC-MS, liquid chromatography−mass spectrometry; LSC, leukemia stem cell; m6A, N6-methyladenosine; m6Am, N6,2′-O-dimethyladenosine; METTL3, Methyltransferase-like 3; METTL14, Methyltransferase-like 14; OA, orotate; SD, standard deviation; RARA, Retinoic Acid Receptor Alpha; TKI, tyrosine kinase inhibitor; UMP, uridine monophosphate

■ REFERENCES

(1) Barbieri, I.; Kouzarides, T. Role of RNA modifications in cancer. *Nat. Rev. Cancer* 2020, 20, 303−322.

(2) Deng, X.; Qing, Y.; Horne, D.; Huang, H.; Chen, J. The roles and implications of RNA m6A modification in cancer. *Nat. Rev. Clin. Oncol.* 2023, 20, 507−526.

(3) Zaccara, S.; Ries, R. J.; Jaffrey, S. R. Reading, writing and erasing mRNA methylation. *Nat. Rev. Mol. Cell Biol.* 2019, 20, 608−624.

(4) Li, Z.; Weng, H.; Su, R.; Weng, X.; Zuo, Z.; Li, C.; Huang, H.; Nachtergaele, S.; Dong, L.; Hu, C.; Qin, X.; Tang, L.; Wang, Y.; Hong, G. M.; Huang, H.; Wang, X.; Chen, P.; Gurbuxani, S.; Arnovitz, S.; Li, Y.; Li, S.; Strong, J.; Neilly, M. B.; Larson, R. A.; Jiang, X.; Zhang, P.; Jin, J.; He, C.; Chen, J. FTO Plays an Oncogenic Role in Acute Myeloid Leukemia as a N6-Methyladenosine RNA Demethylase. *Cancer Cell* 2017, 31, 127−141.

(5) Qing, Y.; Dong, L.; Gao, L.; Li, C.; Li, Y.; Han, L.; Prince, E.; Tan, B.; Deng, X.; Wetzel, C.; Shen, C.; Gao, M.; Chen, Z.; Li, W.; Zhang, B.; Braas, D.; Ten Hoeve, J.; Sanchez, G. J.; Chen, H.; Chan, L. N.; Chen, C. W.; Ann, D.; Jiang, L.; Müschen, M.; Marcucci, G.; Plas, D. R.; Li, Z.; Su, R.; Chen, J. R-2-hydroxyglutarate attenuates aerobic glycolysis in leukemia by targeting the FTO/m6A/PFKP/LDHB axis. *Mol. Cell* 2021, 81, 922−939.e9.

(6) Zhou, W.; Li, S.; Wang, H.; Zhou, J.; Li, S.; Chen, G.; Guan, W.; Fu, X.; Nervi, C.; Yu, L.; Li, Y. A novel AML1-ETO/FTO positive feedback loop promotes leukemogenesis and Ara-C resistance via stabilizing IGFBP2 in t(8;21) acute myeloid leukemia. *Exp. Hematol. Oncol.* 2024, 13, 9.

(7) Yan, F.; Al-Kali, A.; Zhang, Z.; Liu, J.; Pang, J.; Zhao, C.; He, C.; Litzow, M. R.; Liu, S. A dynamic N6-methyladenosine methylome regulates intrinsic and acquired resistance to tyrosine kinase inhibitors. *Cell Res.* 2018, 28, 1062−1076.

(8) Li, Y.; Su, R.; Deng, X.; Chen, Y.; Chen, J. FTO in cancer: functions, molecular mechanisms, and therapeutic implications. *Trends Cancer* 2022, 8, 598−614.

(9) Huang, Y.; Su, R.; Sheng, Y.; Dong, L.; Dong, Z.; Xu, H.; Ni, T.; Zhang, Z. S.; Zhang, T.; Li, C.; Han, L.; Zhu, Z.; Lian, F.; Wei, J.; Deng, Q.; Wang, Y.; Wunderlich, M.; Gao, Z.; Pan, G.; Zhong, D.; Zhou, H.; Zhang, N.; Gan, J.; Jiang, H.; Mulloy, J. C.; Qian, Z.; Chen, J.; Yang, C. G. Small-Molecule Targeting of Oncogenic FTO Demethylase in Acute Myeloid Leukemia. *Cancer Cell* 2019, 35, 677−691.e10.

(10) Su, R.; Dong, L.; Li, Y.; Gao, M.; Han, L.; Wunderlich, M.; Deng, X.; Li, H.; Huang, Y.; Gao, L.; Li, C.; Zhao, Z.; Robinson, S.; Tan, B.; Qing, Y.; Qin, X.; Prince, E.; Xie, J.; Qin, H.; Li, W.; Shen, C.; Sun, J.; Kulkarni, P.; Weng, H.; Huang, H.; Chen, Z.; Zhang, B.; Wu, X.; Olsen, M. J.; Müschen, M.; Marcucci, G.; Salgia, R.; Li, L.; Fathi, A. T.; Li, Z.; Mulloy, J. C.; Wei, M.; Horne, D.; Chen, J. Targeting FTO Suppresses Cancer Stem Cell Maintenance and Immune Evasion. *Cancer Cell* 2020, 38, 79−96.

(11) Ali, E. S.; Ben-Sahra, I. Regulation of nucleotide metabolism in cancers and immune disorders. *Trends Cell Biol.* 2023, 33, 950−966.

(12) Xiao, P.; Duan, Z.; Liu, Z.; Chen, L.; Zhang, D.; Liu, L.; Zhou, C.; Gan, J.; Dong, Z.; Yang, C. G. Rational Design of RNA Demethylase FTO Inhibitors with Enhanced Antileukemia Drug-Like Properties. *J. Med. Chem.* 2023, 66, 9731−9752.

(13) Chen, S. F.; Perrella, F. W.; Behrens, D. L.; Papp, L. M. Inhibition of dihydroorotate dehydrogenase activity by brequinar sodium. *Cancer Res.* 1992, 52, 3521−3527.

(14) Gehlot, P.; Vyas, V. K. A Patent Review of Human Dihydroorotate Dehydrogenase (hDHODH) Inhibitors as Anticancer Agents and their Other Therapeutic Applications (1999−2022). *Recent Pat Anticancer Drug Discovery* 2024, 19, 280−297.

(15) Sykes, D. B.; Kfoury, Y. S.; Mercier, F. E.; Wawer, M. J.; Law, J. M.; Haynes, M. K.; Lewis, T. A.; Schajnovitz, A.; Jain, E.; Lee, D.; Meyer, H.; Pierce, K. A.; Tolliday, N. J.; Waller, A.; Ferrara, S. J.; Eheim, A. L.; Stoeckigt, D.; Maxcy, K. L.; Cobert, J. M.; Bachand, J.; Szekely, B. A.; Mukherjee, S.; Sklar, L. A.; Kotz, J. D.; Clish, C. B.; Sadreyev, R. I.; Clemons, P. A.; Janzer, A.; Schreiber, S. L.; Scadden, D. T. Inhibition of Dihydroorotate Dehydrogenase Overcomes Differentiation Blockade in Acute Myeloid Leukemia. *Cell* 2016, 167, 171−186.

(16) Mauer, J.; Luo, X.; Blanjoie, A.; Jiao, X.; Grozhik, A. V.; Patil, D. P.; Linder, B.; Pickering, B. F.; Vasseur, J. J.; Chen, Q.; Gross, S. S.; Elemento, O.; Debart, F.; Kiledjian, M.; Jaffrey, S. R. Reversible methylation of m6Am in the 5′ cap controls mRNA stability. *Nature* 2021, 541, 371−375.

(17) Relier, S.; Ripoll, J.; Guillorit, H.; Amalric, A.; Achour, C.; Boissière, F.; Vialaret, J.; Attina, A.; Debart, F.; Choquet, A.; Macari, F.; Marchand, V.; Motorin, Y.; Samalin, E.; Vasseur, J. J.; Pannequin, J.; Aguilo, F.; Lopez-Crapez, E.; Hirtz, C.; Rivals, E.; Bastide, A.; David, A. FTO-mediated cytoplasmic m6Am demethylation adjusts stem-like properties in colorectal cancer cell. *Nat. Commun.* 2021, 12, 1716.

(18) Houshmand, M.; Vitale, N.; Orso, F.; Cignetti, A.; Molineris, I.; Gaidano, V.; Sainas, S.; Giorgis, M.; Boschi, D.; Fava, C.; Passoni, A.; Gai, M.; Geuna, M.; Sora, F.; Iurlo, A.; Abruzzese, E.; Breccia, M.; Mulas, O.; Caocci, G.; Castagnetti, F.; Taverna, D.; Oliviero, S.; Pane, F.; Lolli, M. L.; Circosta, P.; Saglio, G. Dihydroorotate dehydrogenase inhibition reveals metabolic vulnerability in chronic myeloid leukemia. *Cell Death Dis.* 2022, 13, 576.

(19) Lafita-Navarro, M. C.; Venkateswaran, N.; Kilgore, J. A.; Kanji, S.; Han, J.; Barnes, S.; Williams, N. S.; Buszczak, M.; Burma, S.; Conacci-Sorrell, M. Inhibition of the de novo pyrimidine biosynthesis pathway limits ribosomal RNA transcription causing nucleolar stress in glioblastoma cells. *PLoS Genet.* 2020, 16, No. e1009117.

(20) So, J.; Lewis, A. C.; Smith, L. K.; Stanley, K.; Franich, R.; Yoannidis, D.; Pijpers, L.; Dominguez, P.; Hogg, S. J.; Vervoort, S. J.; Brown, F. C.; Johnstone, R. W.; McDonald, G.; Ulanet, D. B.; Murtie, J.; Gruber, E.; Kats, L. M. Inhibition of pyrimidine biosynthesis targets protein translation in acute myeloid leukemia. *EMBO Mol. Med.* 2022, 14, No. e15203.

(21) Liu, L.; Mo, W.; Chen, M.; Qu, Y.; Wang, P.; Liang, Y.; Yan, X. Targeted inhibition of DHODH is synergistic with BCL2 blockade in HGBCL with concurrent MYC and BCL2 rearrangement. *BMC Cancer.* 2024, 24, 761.

(22) Kayamori, K.; Nagai, Y.; Zhong, C.; Kaito, S.; Shinoda, D.; Koide, S.; Kuribayashi, W.; Oshima, M.; Nakajima-Takagi, Y.; Yamashita, M.; Mimura, N.; Becker, H. J.; Izawa, K.; Yamazaki, S.; Iwano, S.; Miyawaki, A.; Ito, R.; Tohyama, K.; Lennox, W.; Sheedy, J.; Weetall, M.; Sakaida, E.; Yokote, K.; Iwama, A. DHODH inhibition synergizes with DNA-demethylating agents in the treatment of myelodysplastic syndromes. *Blood Adv.* 2021, 5, 438−450.

(23) Sexauer, A. N.; Alexe, G.; Gustafsson, K.; Zanetakos, E.; Milosevic, J.; Ayres, M.; Gandhi, V.; Pikman, Y.; Stegmaier, K.; Sykes, D. B. DHODH: a promising target in the treatment of T-cell acute lymphoblastic leukemia. *Blood Adv.* 2023, 7, 6685−6701.

(24) Yang, C.; Zhao, Y.; Wang, L.; Guo, Z.; Ma, L.; Yang, R.; Wu, Y.; Li, X.; Niu, J.; Chu, Q.; Fu, Y.; Li, B. De novo pyrimidine biosynthetic complexes support cancer cell proliferation and ferroptosis defence. *Nat. Cell Biol.* 2023, 25, 836−847.

(25) Cao, L.; Weetall, M.; Trotta, C.; Cintron, K.; Ma, J.; Kim, M. J.; Furia, B.; Romfo, C.; Graci, J. D.; Li, W.; Du, J.; Sheedy, J.; Hedrick, J.; Risher, N.; Yeh, S.; Qi, H.; Arasu, T.; Hwang, S.; Lennox, W.; Kong, R.; Petruska, J.; Moon, Y. C.; Babiak, J.; Davis, T. W.; Jacobson, A.; Almstead, N. G.; Branstrom, A.; Colacino, J. M.; Peltz, S. W. Targeting of Hematologic Malignancies with PTC299, A Novel Potent Inhibitor of Dihydroorotate Dehydrogenase with Favorable Pharmaceutical Properties. *Mol. Cancer Ther.* 2019, 18, 3−16.

(26) Peters, G. J.; Schwartsmann, G.; Nadal, J. C.; Laurensse, E. J.; van Groeningen, C. J.; van der Vijgh, W. J.; Pinedo, H. M. In vivo inhibition of the pyrimidine de novo enzyme dihydroorotic acid dehydrogenase by brequinar sodium (DUP-785; NSC 368390) in mice and patients. *Cancer Res.* **1990**, *50*, 4644−4649.

(27) Baumgartner, R.; Walloschek, M.; Kralik, M.; Gotschlich, A.; Tasler, S.; Mies, J.; Leban, J. Dual binding mode of a novel series of DHODH inhibitors. *J. Med. Chem.* **2006**, *49*, 1239−1247.

(28) Lassalas, P.; Gay, B.; Lasfargeas, C.; James, M. J.; Tran, V.; Vijayendran, K. G.; Brunden, K. R.; Kozlowski, M. C.; Thomas, C. J.; Smith, A. B., 3rd; Huryn, D. M.; Ballatore, C. Structure Property Relationships of Carboxylic Acid Isosteres. *J. Med. Chem.* **2016**, *59*, 3183−203.

(29) Moroz-Omori, E. V.; Huang, D.; Kumar Bedi, R.; Cheriyamkunnel, S. J.; Bochenkova, E.; Dolbois, A.; Rzeczkowski, M. D.; Li, Y.; Wiedmer, L.; Caflisch, A. METTL3 Inhibitors for Epitranscriptomic Modulation of Cellular Processes. *ChemMedChem* **2021**, *16*, 3035−3043.

(30) Ianniello, Z.; Sorci, M.; Ceci Ginistrelli, L.; Iaiza, A.; Marchioni, M.; Tito, C.; Capuano, E.; Masciarelli, S.; Ottone, T.; Attrotto, C.; Rizzo, M.; Franceschini, L.; de Pretis, S.; Voso, M. T.; Pelizzola, M.; Fazi, F.; Fatica, A. New insight into the catalytic -dependent and -independent roles of METTL3 in sustaining aberrant translation in chronic myeloid leukemia. *Cell Death Dis.* **2021**, *12*, 870.

(31) Proietti, L.; Manhart, G.; Heyes, E.; Troester, S.; Grebien, F. Arrayed CRISPR/Cas9 Screening for the Functional Validation of Cancer Genetic Dependencies. *Bio Protoc.* **2022**, *12*, No. e4577.

(32) Sanjana, N. E.; Shalem, O.; Zhang, F. Improved vectors and genome-wide libraries for CRISPR screening. *Nat. Methods* **2014**, *11*, 783−784.

(33) Love, M. I.; Huber, W.; Anders, S. Moderated estimation of fold change and dispersion for RNA-seq data with DESeq2. *Genome Biol.* **2014**, *15*, 550.

(34) Xie, Z.; Bailey, A.; Kuleshov, M. V.; Clarke, D. J. B.; Evangelista, J. E.; Jenkins, S. L.; Lachmann, A.; Wojciechowicz, M. L.; Kropiwnicki, E.; Jagodnik, K. M.; Jeon, M.; Ma'ayan, A. Gene Set Knowledge Discovery with Enrichr. *Curr. Protoc.* **2021**, *1*, No. e90.

(35) Rosignoli, S.; Paiardini, A. DockingPie: a consensus docking plugin for PyMOL. *Bioinformatics* **2022**, *38*, 4233−4234.

(36) Sainas, S.; Pippione, A. C.; Giorgis, M.; Lupino, E.; Goyal, P.; Ramondetti, C.; Buccinnà, B.; Piccinini, M.; Braga, R. C.; Andrade, C. H.; Andersson, M.; Moritzer, A. C.; Friemann, R.; Mensa, S.; Al-Kadaraghi, S.; Boschi, D.; Lolli, M. L. Design, synthesis, biological evaluation and X-ray structural studies of potent human dihydroorotate dehydrogenase inhibitors based on hydroxylated azole scaffolds. *Eur. J. Med. Chem.* **2017**, *129*, 287−302.

(37) Martinez Molina, D.; Jafari, R.; Ignatushchenko, M.; Seki, T.; Larsson, E. A.; Dan, C.; Sreekumar, L.; Cao, Y.; Nordlund, P. Monitoring drug target engagement in cells and tissues using the cellular thermal shift assay. *Science* **2013**, *341*, 84−87.